Supplementary Information for "Observation of measurement-induced entanglement and quantum trajectories of remote superconducting qubits"

Nicolas Roch*†,[1] Mollie E. Schwartz*,[1] Felix Motzoi,[2] Christopher Macklin,[1] Rajamani Vijay,[3] Andrew W. Eddins,[1] Alexander N. Korotkov,[4] Birgitta Whaley,[2] Mohan Sarovar,[5] and Irfan Siddiqi[1]

[1] *Quantum Nanoelectronics Laboratory, Department of Physics, University of California, Berkeley, California 94720, USA.*
[2] *Department of Chemistry, University of California, Berkeley, California 94720, USA.*
[3] *Department of Condensed Matter Physics and Materials Science, Tata Institute of Fundamental Research, Mumbai,400005, India.*
[4] *Department of Electrical Engineering, University of California, Riverside, California 92521, USA.*
[5] *Scalable and Secure Systems Research (08961), Sandia National Laboratories, Livermore, CA 94550, USA*

* These authors contributed equally to this work
† Present address: CNRS and Université Grenoble Alpes, Institut Néel, 38042 Grenoble, France

SIMPLIFIED THEORY

In this section we describe a simplified phenomenological theory for calculation of the concurrence in our experiment. This theory is not intended to give a rigorously accurate result, but can be used for quick estimates and for gaining physical intuition. For clarity, we use $A(t)$ and $B(t)$ to represent the intracavity fields in cavity 1 and cavity 2, respectively, and A_{out}, B_{out} to represent the propagating fields travelling *from* the respective cavities.

For simplicity we neglect the off-diagonal elements $\rho_{00,01}$, $\rho_{00,10}$, $\rho_{11,01}$, and $\rho_{11,10}$ of the two-qubit density matrix (which should be small in the interesting regime – see below), so that we have the so-called X-state and therefore can use the simplified formula [1] for the concurrence,

$$\mathcal{C} = 2\max(0, |\rho_{01,10}| - \sqrt{\rho_{00,00}\rho_{11,11}}), \tag{1}$$

which depends only on two diagonal elements and one off-diagonal element of the density matrix. (This concurrence does not depend on the element $\rho_{11,00}$, so we do not have to neglect it; however, in experiment it is even smaller than the neglected elements.)

To find $\rho_{00,00}$, $\rho_{11,11}$, and $\rho_{01,10}$ after the measurement, we first consider the case without energy relaxation and intrinsic (not measurement-induced) dephasing of the qubits; then the dynamics of the two-qubit state are only due to measurement. For each of four "classical" initial states of the qubits ($|00\rangle$, $|01\rangle$, $|10\rangle$, $|11\rangle$) it is easy to calculate the evolution of the classical field amplitudes $A(t)$ and $B(t)$ in the first and second resonators,

$$\dot{A} = -\frac{\kappa_1}{2}A - i(\omega_{r,1} \pm \chi_1 - \omega_m)A + \sqrt{\kappa_{s,1}}\, A_d(t), \tag{2}$$

$$\dot{B} = -\frac{\kappa_2}{2}B - i(\omega_{r,2} \pm \chi_2 - \omega_m)B + \sqrt{\kappa_{s,2}}\sqrt{\eta_{loss}}\, A_{out}(t), \tag{3}$$

As in the main text, + (−) refers to the qubit state $|0\rangle$ ($|1\rangle$). Here the rotating frame ($e^{-i\omega_m t}$) is based on the measurement drive, the time for $B(t)$ is shifted by the "flying time" between resonators, $A_d(t)$ is the external microwave drive amplitude (α_{in} in the main paper, $\kappa_1 = \kappa_{s,1} + \kappa_{w,1} + \kappa_{decay,1}$ is the total bandwidth of the first resonator (including the bandwidth due to strongly and weakly coupled ports —see Fig.1), and similarly $\kappa_2 = \kappa_{s,2} + \kappa_{w,2} + \kappa_{decay,2}$ for the second resonator. The energy decay for the microwave propagation *between* the resonators is described by the efficiency η_{loss}, which describes the losses in the circulator and microwave cables. Notice that in Eqs. (2) and (3) the resonator field amplitudes A and B are normalized such that $|A|^2$ and $|B|^2$ are equal to the average number of photons in the corresponding coherent states, while for the propagating field A_d the squared amplitude $|A_d|^2$ is equal to the average number of photons per unit time.

Similar normalization is used for the propagating field

$$A_{out}(t) = -A_d(t) + \sqrt{\kappa_{s,1}}\, A(t), \tag{4}$$

and the field

$$B_{out}(t) = -\sqrt{\eta_{loss}}\, A_{out}(t) + \sqrt{\kappa_{s,2}}\, B(t), \tag{5}$$

which goes from the second resonator through the circulator to the amplifier. In the steady-state limit ($\dot{A} = 0$) and for $\kappa_s \gg \kappa_w + \kappa_{decay}$, we recover the experessions given in the main paper for the reflection coefficient:

$$r^{\pm} = \frac{\kappa_s - 2i(\omega_r - \omega_m \pm \chi)}{\kappa_s + 2i(\omega_r - \omega_m \pm \chi)}, \tag{6}$$

and for the photon number population inside cavity 1:

$$\bar{n}_1^{\pm} = \frac{\kappa_{s,1}}{(\kappa_{s,1}/2)^2 + (\omega_1 - \omega_m \pm \chi_1)^2}\, |A_d|^2 . \tag{7}$$

To produce the entangled state in our experiment, the steady-state fields $B_{out}^{(01)}$ and $B_{out}^{(10)}$ for the states $|01\rangle$ and $|10\rangle$ should be indistinguishable, $B_{out}^{(01)} = B_{out}^{(10)}$, while they should be sufficiently well distinguishable from the fields $B_{out}^{(00)}$ and $B_{out}^{(11)}$. For amplification and homodyne measurement of the field quadrature $e^{i\phi}$, the average time-integrated measurement result for the state $|ij\rangle$ is

$$S_{ij} = \frac{1}{t} \int \mathrm{Re}[B_{out}^{(ij)}(t')\, e^{-i\phi}]\, f_w(t')\, dt', \tag{8}$$

where $f_w(t)$ is the weight function (in the experiment we used constant-weight integration with adjustable start/end time moments). The amplifier noise is also accumulated during this time-integration, so that for the two-qubit state $|ij\rangle$ the random measurement result is characterized by the Gaussian distribution with the mean value of S_{ij} and the standard deviation

$$\sigma = \frac{1}{2\sqrt{\eta_{meas}}} \sqrt{\frac{1}{t} \int f_w^2(t)\, dt}, \tag{9}$$

where η_{meas} is the quantum efficiency of the measurement setup, which includes quantum efficiency of the phase-sensitive amplifier and losses in the circulators and cables. Notice that the noise σ does not depend on the two-qubit state. In our experiment $\eta_{meas} = 0.4$, $\eta_{loss} = 0.75$, and the measured phase ϕ is chosen to be perpendicular to the output states for $|01\rangle$ and $|10\rangle$, $\phi = \arg(B_{out}^{(10)}) = \arg(B_{out}^{(01)})$.

In the experiment we select only realizations for which the integrated signal falls within a certain range, centered near $(S_{01} + S_{10})/2$. The total probability of selection in our model (assuming no energy relaxation of qubits) is then

$$p_{ent} = \sum_{i,j} \rho_{ij,ij}^{in}\, p_{sel}(i,j), \tag{10}$$

where ρ^{in} is the two-qubit density matrix before the measurement and $p_{sel}(i,j)$ is the selection probability for the initial state $|ij\rangle$ (it is equal to the integral, within the selection range, of the Gaussian with mean value S_{ij} and standard deviation σ). In the experiment the selection range is typically chosen to keep 10% of realizations, $p_{ent} = 0.1$.

Since the two-qubit state evolution is only due to measurement, the diagonal matrix elements of the final density matrix ρ^{fin} should obey [2] the classical Bayes rule

$$\rho_{ij,ij}^{fin} = \frac{\rho_{ij,ij}^{in}\, p_{sel}(i,j)}{p_{ent}}. \tag{11}$$

For the main off-diagonal matrix element $\rho^{fin}_{01,10}$ needed to calculate concurrence, the quantum Bayesian approach [2] cannot be applied rigorously; however, we can modify it phenomenologically by using the following approximation:

$$
\begin{aligned}
|\rho^{fin}_{01,10}| = |\rho^{in}_{01,10}| \, & \frac{\sqrt{\rho^{fin}_{01,01}\rho^{fin}_{10,10}}}{\sqrt{\rho^{in}_{01,01}\rho^{in}_{10,10}}} \\
& \times \exp\left[-\frac{1}{2}\int |B^{(01)}_{out}(t) - B^{(10)}_{out}(t)|^2 dt\right] \\
& \times \exp\left[-\frac{1}{2}\int \left((1-\eta_{loss})\,\kappa_{s,1} + \kappa_{w,1} + \kappa_{decay,1}\right) |A^{(01)}(t) - A^{(10)}(t)|^2 dt\right] \\
& \times \exp\left[-\frac{1}{2}\int \left(\kappa_{w,2} + \kappa_{decay,2}\right) |B^{(01)} - B^{(10)}|^2 dt\right], \qquad (12)
\end{aligned}
$$

where the last three factors describe the dephasing due to potential distinguishability of states $|01\rangle$ and $|10\rangle$ in the field B_{out} and "lost" fractions of the fields A and B from the first and second resonators. The form of these dephasing factors directly follows from the overlap between two coherent states $|A_1\rangle$ and $|A_2\rangle$ in a resonator [3]: $|\langle A_1|A_2\rangle| = \exp(-|A_1 - A_2|^2/2)$.

Only the absolute value of $\rho^{fin}_{01,10}$ is needed to calculate the concurrence (1). For completeness, the phase change of $\rho_{01,10}$ due to measurement can be approximately calculated using the master equation result [4]

$$
\arg(\rho^{fin}_{01,10}) - \arg(\rho^{in}_{01,10}) = 2\chi_1 \int \mathrm{Re}[A^{(01)}(t)A^{(10)}(t)^*]\, dt - 2\chi_2 \int \mathrm{Re}[B^{(01)}(t)B^{(10)}(t)^*]\, dt. \qquad (13)
$$

(Here we used a frame that takes care of unequal bare frequencies of the qubits.)

Now let us discuss the density matrix element $\rho^{fin}_{00,01}$, which was neglected in the calculation of concurrence (1). Very crudely, it can be estimated as $|\rho^{fin}_{00,01}| \lesssim \sqrt{\rho^{fin}_{00,00}\rho^{fin}_{01,01}}\, \exp[-\frac{1}{2}(1-\eta_{meas}) \int |B^{(00)}_{out} - B^{(01)}_{out}|^2\, dt]$, where the exponential term is due to the "unmeasured" part of B_{out}. In the interesting regime (when a significant entanglement is achieved) we have $\rho^{fin}_{00,00} \ll 1$ and the exponential term is also small because distinguishability of the states $|00\rangle$ and $|01\rangle$ is governed by a similar factor. This is why $\rho^{fin}_{00,01}$ is strongly suppressed, and we believe it can be neglected in approximate calculation of concurrence. Similar arguments can be used to show strong suppression of the density matrix elements $\rho^{fin}_{00,10}$, $\rho^{fin}_{11,01}$, and $\rho^{fin}_{11,10}$ in the regime interesting for producing significant entanglement.

So far we have assumed absence of intrinsic decoherence of the qubits. Pure dephasing of the qubits with the corresponding dephasing time $T_{\varphi,1}$ and $T_{\varphi,2}$ can be easily included into the calculation of concurrence by multiplying the main off-diagonal element $\rho^{fin}_{01,10}$ by the factor $\exp(-t_m/T_{\varphi,1} - t_m/T_{\varphi,2})$, where t_m is the total duration of the measurement procedure. Including the energy relaxation is not so easy, but since its contribution is quite small in the experiment, this can be done in a very crude way. For example, instead of the energy relaxation occuring during the measurement, we can phenomenologically introduce the energy relaxation for time t_{before} before the measurement and then for time t_{after} after the measurement. A better way can be realized by assuming energy decay at a specific random time, and then adding two corresponding parts of the signal integration (8); however, this complication does not seem necessary for our simplified theory.

THEORETICAL MODEL BASED ON QUANTUM TRAJECTORY THEORY

A sequential probe of two cavities as in Fig. 1a of the main text is often referred to as a cascaded systems setup, and Carmichael [7] has developed the quantum trajectory equations describing such one-way sequential probes of cascaded systems. Following this work we can write a stochastic master equation (SME) model for the experimental

setup that includes qubit and cavity degrees of freedom:

$$\begin{aligned}\frac{\mathrm{d}\rho}{\mathrm{d}t} &= -i[H,\rho] + \mathcal{D}[\sqrt{\kappa_{\mathrm{s},1}(1-\eta_{loss})}a]\rho + \mathcal{D}[-\sqrt{\kappa_{\mathrm{s},1}\eta_{loss}}a + \sqrt{\kappa_{\mathrm{s},2}}b]\rho + \kappa_{\mathrm{w},1}\mathcal{D}[a]\rho + \kappa_{\mathrm{w},2}\mathcal{D}[b]\rho \\ &+\sqrt{\eta_{\mathrm{meas}}}\xi(t)\mathcal{H}[e^{i\phi}(-\sqrt{\kappa_{\mathrm{s},1}\eta_{loss}}a + \sqrt{\kappa_{\mathrm{s},2}}b)]\rho \\ &+\sum_{i=1}^{2}\Gamma_{\varphi}^{i}\mathcal{D}[\sigma_z^i]\rho + \sum_{i=1}^{2}\Gamma_{r}^{i}\mathcal{D}[\sigma_-^i]\rho \end{aligned} \tag{14}$$

with variables as defined in the previous section. This equation is in Ito form and therefore $\xi(t)dt = dW(t)$. $dW(t)$ is a Wiener increment satisfying $E\{dW(t)\} = 0$ and $E\{dW(t)dW(s)\} = \delta(t-s)$ ($E\{\cdot\}$ denotes expectation value). $a(b)$ is an annihilation operator for the intracavity field in cavity 1 (2). $\sigma_\alpha^{1(2)}$ is the α Pauli operator for qubit 1 (2). The superoperators above are defined as: $\mathcal{D}[A]B \equiv ABA^\dagger - \frac{1}{2}A^\dagger AB - \frac{1}{2}BA^\dagger A$ and $\mathcal{H}[A]B \equiv AB + BA^\dagger - \mathrm{tr}\,(AB+BA^\dagger)B$. The last line in this equation is the dephasing and relaxation of the qubits, and we assume these are described by Markovian processes – *e.g.*, $\Gamma_r^i = 1/T_1^i$. This equation describes the conditioned state of the system under a measurement voltage trace

$$V(t) = \sqrt{\eta_{\mathrm{meas}}}\langle -\sqrt{\kappa_{\mathrm{s},1}\eta_{loss}}a + \sqrt{\kappa_{\mathrm{s},2}}b\rangle + \xi(t) \tag{15}$$

The observable that is being monitored is $-\sqrt{\kappa_{\mathrm{s},1}\eta_{loss}}a + \sqrt{\kappa_{\mathrm{s},2}}b$ in terms of the intra-cavity field operators. Note that an equivalent way to write the above SME is to replace $\xi(t)$ with the quantity $V(t) - \sqrt{\eta_{\mathrm{meas}}}\langle -\sqrt{\kappa_{\mathrm{s},1}\eta_{loss}}a + \sqrt{\kappa_{\mathrm{s},2}}b\rangle$, which is the difference between what is measured and the best estimate of the observable.

The transmission time between the two cavities is taken to be negligible and therefore a direct coupling effective Hamiltonian between intracavity fields can be derived using the methods in [7]. This effective Hamiltonian is

$$\begin{aligned}H &= -\frac{\omega_{q,1}}{2}\sigma_z^1 - \frac{\omega_{q,2}}{2}\sigma_z^2 + \omega_{r,1}a^\dagger a + \omega_{r,2}b^\dagger b + \chi_1 a^\dagger a\sigma_z^1 + \chi_2 b^\dagger b\sigma_z^2 \\ &-i\frac{\sqrt{\kappa_{\mathrm{s},1}\kappa_{\mathrm{s},2}\eta_{loss}}}{2}(a^\dagger b - b^\dagger a) + iA_d(t)\sqrt{\kappa_{\mathrm{w},1}}a^\dagger - iA_d^*(t)\sqrt{\kappa_{\mathrm{w},1}}a \end{aligned} \tag{16}$$

where $\omega_{q,i}$ is the qubit transition frequency. This Hamiltonian is in the rotating frame with respect to the measurement tone frequency – i.e rotating frame with respect to $H_0 = \omega_m a^\dagger a + \omega_m b^\dagger b$. The coupling between cavities is mediated by a propagating field and therefore is irreversible. The combination of the Hamiltonian and dissipative components of Eq. (14) result in a unidirectional coupling, as will be seen below.

In the following we do not consider driving of the qubit states and assume that the qubit states are σ_x eigenstates at $t = 0$. Simultaneous modeling of the projective dynamics of the measurement and qubit driving is challenging and must be done by a careful adiabatic elimination [8, 9]. We find that modeling the additional dynamics introduced by the interplay of these two aspects is not necessary to get a good match to experiment and therefore consider a perfectly prepared initial state.

The Heisenberg equations of motion for expected values of the intra-cavity fields under unconditioned evolution (the unconditioned/average evolution is the same as Eq. (14) but without the stochastic last term) are:

$$\langle\dot{a}\rangle = -i\omega_{r,1}\langle a\rangle - i\chi_1\langle\sigma_z^a a\rangle - \frac{\kappa_{\mathrm{s},1}+\kappa_{\mathrm{w},1}}{2}\langle a\rangle + A_d(t)\sqrt{\kappa_{\mathrm{w},1}} \tag{17}$$

$$\langle\dot{b}\rangle = -i\omega_{r,2}\langle b\rangle - i\chi_2\langle\sigma_z^b b\rangle - \frac{\kappa_{\mathrm{s},2}+\kappa_{\mathrm{w},2}}{2}\langle b\rangle + \sqrt{\kappa_{\mathrm{s},1}\kappa_{\mathrm{s},2}\eta_{loss}}\langle a\rangle \tag{18}$$

These evolution equations make explicit the fact that the second cavity is driven by the first but not vice-versa. From these equations we can write evolution equations for coherent states of the intra-cavity fields conditioned on the qubits

being in given states:

$$\begin{aligned}
\dot{A}^{(0)} &= -i\omega_{r,1}A^{(0)} - i\chi_1 A^{(0)} - \frac{\kappa_{\mathrm{s},1}+\kappa_{\mathrm{w},1}}{2}A^{(0)} + A_d(t)\sqrt{\kappa_{\mathrm{s},1}} \\
\dot{A}^{(1)} &= -i\omega_{r,1}A^{(1)} + i\chi_1 A^{(1)} - \frac{\kappa_{\mathrm{s},1}+\kappa_{\mathrm{w},1}}{2}A^{(1)} + A_d(t)\sqrt{\kappa_{\mathrm{s},1}} \\
\dot{B}^{(11)} &= -i\omega_{r,2}B^{(11)} + i\chi_2 B^{(11)} - \frac{\kappa_{\mathrm{s},2}+\kappa_{\mathrm{w},2}}{2}B^{(11)} + \sqrt{\kappa_{\mathrm{s},1}\kappa_{\mathrm{s},2}\eta_{loss}}\ A^{(1)} \\
\dot{B}^{(10)} &= -i\omega_{r,2}B^{(10)} - i\chi_2 B^{(10)} - \frac{\kappa_{\mathrm{s},2}+\kappa_{\mathrm{w},2}}{2}B^{(10)} + \sqrt{\kappa_{\mathrm{s},1}\kappa_{\mathrm{s},2}\eta_{loss}}\ A^{(1)} \\
\dot{B}^{(01)} &= -i\omega_{r,2}B^{(01)} + i\chi_2 B^{(01)} - \frac{\kappa_{\mathrm{s},2}+\kappa_{\mathrm{w},2}}{2}B^{(01)} + \sqrt{\kappa_{\mathrm{s},1}\kappa_{\mathrm{s},2}\eta_{loss}}\ A^{(0)} \\
\dot{B}^{(00)} &= -i\omega_{r,2}B^{(00)} - i\chi_2 B^{(00)} - \frac{\kappa_{\mathrm{s},2}+\kappa_{\mathrm{w},2}}{2}B^{(00)} + \sqrt{\kappa_{\mathrm{s},1}\kappa_{\mathrm{s},2}\eta_{loss}}\ A^{(0)}
\end{aligned} \tag{19}$$

where $A = \langle a \rangle, B = \langle b \rangle$ and the superscripts indicate the conditioning on qubit states. The state of the second cavity is conditioned on the states of both qubits but the state of the first cavity is only conditioned on the first qubit state since there is no information flowing from the second to the the first cavity. In other words, $A^{(11)} = A^{(10)} = A^{(1)}$ and $A^{(01)} = A^{(00)} = A^{(0)}$. The probe field "bounces" off both cavities and the resulting output field that is measured, in terms of these intra-cavity fields, is:

$$B_{out}(t) = -\sqrt{\kappa_{s,1}\eta_{loss}}A(t) + \sqrt{\kappa_{s,2}}B(t) \tag{20}$$

In Ref. [9] we generalize the techniques developed for a single qubit in a cavity in Ref. [8] to the case relevant here of two cavities with embedded qubits. This generalization allows us to eliminate the cavity degrees of freedom and obtain an equation of motion just for the qubits that aids in assessing the performance of the remote entanglement scheme. However, for the purposes of modeling the present experiment we only detail part of the calculation.

The dynamical equation in Eq. (14) is sufficient to model the experiment, however it is difficult to simulate since it involves both qubit and cavity degrees of freedom. Instead, we will derive an effective SME for the qubit degrees of freedom only. The first step is to perform a polaron transformation into a frame where the average state of both cavities is the vacuum. The correct transform in this two cavity case is $\rho^P(t) = U(t)^\dagger \rho(t) U(t)$, with

$$\begin{aligned}
U(t) &= \Pi_{11} D_1\left[A^{(1)}(t)\right] D_2\left[B^{(11)}(t)\right] + \Pi_{10} D_1\left[A^{(1)}(t)\right] D_2\left[B^{(10)}(t)\right] \\
&\quad + \Pi_{01} D_1\left[A^{(0)}(t)\right] D_2\left[B^{(01)}(t)\right] + \Pi_{00} D_1\left[A^{(0)}(t)\right] D_2\left[B^{(00)}(t)\right]
\end{aligned} \tag{21}$$

where $\Pi_{ij} = |i\rangle_1 \langle i| \otimes |j\rangle_2 \langle j|$ are projectors onto qubit states and $D_{1(2)}[X]$ is a displacement operator for cavity field 1(2) by coherent state X. In this frame, the equation of motion (for an unnormalized density matrix in the polaron frame) becomes

$$\begin{aligned}
\frac{\mathrm{d}\rho^P}{\mathrm{d}t} &= -i[H^P + \frac{i\sqrt{\kappa_{\mathrm{w},1}}}{2}A_d^*(t)\Pi_a - \frac{i\sqrt{\kappa_{\mathrm{w},1}}}{2}A_d(t)\Pi_a^\dagger] \\
&\quad + \mathcal{D}[\sqrt{\kappa_{\mathrm{s},1}(1-\eta_{loss})}a]\rho^P + \mathcal{D}[-\sqrt{\kappa_{\mathrm{s},1}\eta_{loss}}a + \sqrt{\kappa_{\mathrm{s},2}}b]\rho^P + \kappa_{\mathrm{w},1}\mathcal{D}[a]\rho^P + \kappa_{\mathrm{w},2}\mathcal{D}[b]\rho^P \\
&\quad + \mathcal{D}[\sqrt{\kappa_{\mathrm{s},1}(1-\eta_{loss})}\Pi_a]\rho^P + \mathcal{D}[-\sqrt{\kappa_{\mathrm{s},1}\eta_{loss}}\Pi_a + \sqrt{\kappa_{\mathrm{s},2}}\Pi_b]\rho^P + \kappa_{\mathrm{w},1}\mathcal{D}[\Pi_a]\rho^P + \kappa_{\mathrm{w},2}\mathcal{D}[\Pi_b]\rho^P \\
&\quad + \Gamma_1\big(a[\rho^P, \Pi_a^\dagger] + [\Pi_a, \rho^P]a^\dagger\big) + \Gamma_2\big(b[\rho^P, \Pi_b^\dagger] + [\Pi_b, \rho^P]b^\dagger\big) \\
&\quad + \sqrt{\kappa_{\mathrm{s},1}\kappa_{\mathrm{s},2}\eta_{loss}}\big(a[\rho^P, \Pi_b^\dagger] + [\Pi_b, \rho^P]a^\dagger + b[\rho^P, \Pi_a^\dagger] + [\Pi_a, \rho^P]b^\dagger\big) \\
&\quad + \sqrt{\eta_{\mathrm{meas}}}V(t)\bar{\mathcal{H}}[-\sqrt{\kappa_{\mathrm{s},1}\eta_{loss}}a + \sqrt{\kappa_{\mathrm{s},2}}b]\rho^P + \sqrt{\eta_{\mathrm{meas}}}V(t)\bar{\mathcal{H}}[-\sqrt{\kappa_{\mathrm{s},1}\eta_{loss}}\Pi_a + \sqrt{\kappa_{\mathrm{s},2}}\Pi_b]\rho^P \\
&\quad + \sum_{i=a,b}\Gamma_\varphi^i\mathcal{D}[\sigma_z^i]\rho + \sum_{i=a,b}\Gamma_r^i\mathcal{D}[\sigma_-^i]\rho
\end{aligned} \tag{22}$$

where $\bar{\mathcal{H}}[A]B \equiv AB + BA^\dagger$, $\Gamma_{1(2)} =\equiv \kappa_{\mathrm{s},1(2)} + \kappa_{\mathrm{w},1(2)}$ and the projectors are

$$\Pi_a \equiv (\Pi_{10} + \Pi_{11})A^{(1)}(t) + (\Pi_{00} + \Pi_{01})A^{(0)}(t), \qquad \Pi_b \equiv \Pi_{11}B^{(11)}(t) + \Pi_{10}B^{(10)}(t) + \Pi_{01}B^{(01)}(t) + \Pi_{00}B^{(00)}(t) \tag{23}$$

and the Hamiltonian is

$$H^P = -\frac{\omega_{q,1}}{2}\sigma_z^1 - \frac{\omega_{q,2}}{2}\sigma_z^2 + \omega_{r,1}a^\dagger a + \omega_{r,2}b^\dagger b + \chi_1 a^\dagger a\sigma_z^1 + \chi_2 b^\dagger b\sigma_z^2 \tag{24}$$

Notice that in this frame there is no drive of the cavity modes because we are dynamically shifting the cavity states back to the vacuum. Therefore, if the cavity starts off in the vacuum state it always remains in the vacuum state in this frame. This makes simulation of the system much easier since we can drop all the terms above that contain a field operator (notice that all field operators in the dynamical equation are normally ordered so that they annihilate the vacuum). This leaves us with an equation of motion just for the qubits that we can normalize and simulate efficiently. However, at the final time we must transform back into the lab frame from the polaron frame in order to interpret the results consistently. This transformation can be calculated easily by noting that $\rho(t) = U^\dagger(t)\rho^P(t)U(t)$. Consider a general state in the polaron frame:

$$\varrho^P(t) = \sum_{ijkl} r_{ijkl}(t)\left|ij\right\rangle_q\left\langle kl\right| \otimes \left|00\right\rangle_c\left\langle 00\right| \tag{25}$$

where the first two components are qubit states (indicated by the subscript q) and the second two components are the cavity states (indicated by the subscript c). As before we can assume that in the polaron frame the cavity states remain the vacuum. We want to transform back into the lab frame and then trace over the cavity states. That is,

$$\rho(t) = \mathrm{tr}_c\left(U(t)\rho^P(t)U^\dagger(t)\right) \tag{26}$$

where the trace is over cavities 1 and 2. Since in the current work the cavities at at their steady states at the "final time" (when the state characterization is done), we will specialize to the case where the operator $U(t) \to U_{ss}$ is time-independent because the states $A^{(i)}$ and $B^{(ij)}$ are in their steady state (which we indicate by dropping the time index). In this case,

$$\begin{aligned}
\rho(t) &= \mathrm{tr}_c\left(U_{ss}\rho^P(t)U_{ss}^\dagger\right) = \sum_{ijkl} r_{ijkl}(t)\mathrm{tr}\left(U_{ss}\left|ij\right\rangle_q\left\langle kl\right| \otimes \left|00\right\rangle_c\left\langle 00\right|U_{ss}^\dagger\right) \\
&= r_{1111}(t)\left|11\right\rangle_q\left\langle 11\right| + r_{1010}(t)\left|10\right\rangle_q\left\langle 10\right| + r_{0101}(t)\left|01\right\rangle_q\left\langle 01\right| + r_{0000}(t)\left|00\right\rangle_q\left\langle 00\right| \\
&+ \Big\{ r_{1110}(t)_c\left\langle 00\right|D_1^\dagger\left[A^{(1)}\right]D_2^\dagger\left[B^{(10)}\right]D_1\left[A^{(1)}\right]D_2\left[B^{(11)}\right]\left|00\right\rangle_c\left|11\right\rangle_q\left\langle 10\right| + \\
&\quad r_{1101}(t)_c\left\langle 00\right|D_1^\dagger\left[A^{(0)}\right]D_2^\dagger\left[B^{(01)}\right]D_1\left[A^{(1)}\right]D_2\left[B^{(11)}\right]\left|00\right\rangle_c\left|11\right\rangle_q\left\langle 01\right| + \\
&\quad r_{1100}(t)_c\left\langle 00\right|D_1^\dagger\left[A^{(0)}\right]D_2^\dagger\left[B^{(00)}\right]D_1\left[A^{(1)}\right]D_2\left[B^{(11)}\right]\left|00\right\rangle_c\left|11\right\rangle_q\left\langle 00\right| + \\
&\quad r_{1001}(t)_c\left\langle 00\right|D_1^\dagger\left[A^{(0)}\right]D_2^\dagger\left[B^{(01)}\right]D_1\left[A^{(1)}\right]D_2\left[B^{(10)}\right]\left|00\right\rangle_c\left|10\right\rangle_q\left\langle 01\right| + \\
&\quad r_{1000}(t)_c\left\langle 00\right|D_1^\dagger\left[A^{(0)}\right]D_2^\dagger\left[B^{(00)}\right]D_1\left[A^{(1)}\right]D_2\left[B^{(10)}\right]\left|00\right\rangle_c\left|10\right\rangle_q\left\langle 00\right| + \\
&\quad r_{0100}(t)_c\left\langle 00\right|D_1^\dagger\left[A^{(0)}\right]D_2^\dagger\left[B^{(00)}\right]D_1\left[A^{(0)}\right]D_2\left[B^{(01)}\right]\left|00\right\rangle_c\left|01\right\rangle_q\left\langle 00\right| + h.c.\Big\}
\end{aligned} \tag{27}$$

So we see that the diagonal elements are not effected by the transformation back to the lab frame, but that the off-diagonal elements are all scaled by additional factors. These factors can be easily worked out for steady state values of the cavity fields, for example,

$$\left\langle 00\right|D_1^\dagger\left[A^{(0)}\right]D_2^\dagger\left[B^{(01)}\right]D_1\left[A^{(1)}\right]D_2\left[B^{(11)}\right]\left|00\right\rangle = \exp\left\{i\mathrm{Im}\{A^{(0)*}A^{(1)}\} + i\mathrm{Im}\{B^{(01)*}B^{(11)}\} - \frac{|\delta_{10}|^2}{2} - \frac{|\Delta_{1101}|^2}{2}\right\} \tag{28}$$

where $\delta_{ij} \equiv A^{(i)} - A^{(j)}$ and $\Delta_{ijkl} \equiv B^{(ij)} - B^{(kl)}$. So we can propagate the system in the polaron frame (which is more efficient since the cavity states stay at the vacuum) and then at the end scale the off-diagonal elements to get the density matrix in the lab frame.

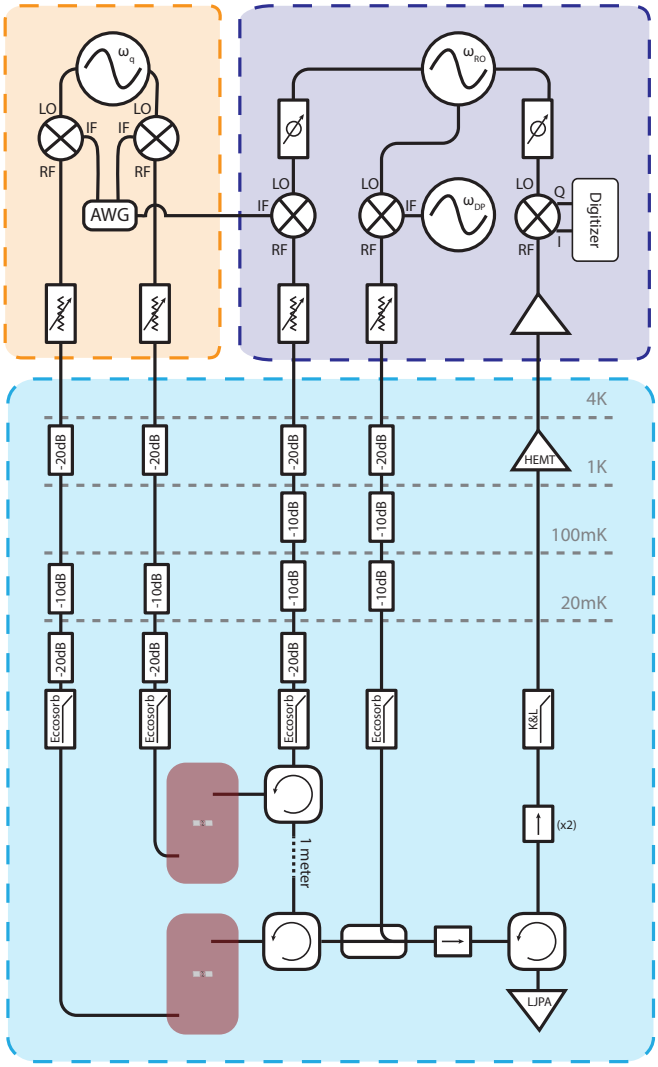

Fig S 1: Full experimental setup.

FULL DETAILS OF EXPERIMENTAL SETUP

The joint measurement process described in this Letter requires the use of two GHz microwave generators (to act as local oscillators for qubit and readout pulses); one MHz generator (for double-pumping the lumped-element Josephson parametric amplifier, LJPA); three DC current sources (for biasing the qubits and the amplifier); and an arbitrary waveform generator (AWG, for shaping qubit and readout pulses). The full room- and base-temperature setup is shown in Figure 1. The qubits are housed at the base stage of a Vericold cryogen-free dilution refrigerator. Input lines contain 50-60 dB of attenuation and additional homemade lossy Eccosorb low-pass filters at base stage to filter stray infrared radiation. The qubits and cavities are housed in a blackened copper can, and the cavities are themselves indium-sealed to provide additional infrared shielding. Magnetic shielding is provided by wrapping the cavities individually with aluminum foil and by a μ-metal outer shield that encompasses the copper can.

To implement qubit pulses, the qubits are first tuned to an operating frequency of $\omega_{q,1}/2\pi = 4.31143$ GHz and

$\omega_{q,2}/2\pi = 4.46143$ GHz. Qubit pulses are implemented using single-sideband modulators (SSBs) with the output of a first generator operating at the midpoint of the two qubit frequencies $\omega_q/2\pi = 4.38643$ GHz serving as the local oscillator (LO). The AWG provides intermediate frequency (IF) pulses at 75 MHz to a lower-sideband SSB (qubit 1) and an upper-sideband SSB (qubit 2); these pulses are routed to base and perform single qubit gates via the weakly-coupled ports of the respective cavities.

A second generator operating at the measurement frequency $\omega_m/2\pi = 7.19326$ GHz is split three ways. The joint measurement readout pulses are implemented via a mixer using ω_m as the LO and DC pulses from the AWG as the IF. The ouput of the mixer passes through a variable phase shift and attenuation and into the dilution refrigerator. At base, the readout passes through a circulator to measure cavity 1 in reflection; is routed back through the circulator and through 1.3 meters of copper cable; measures cavity 2 in reflection via a second circulator; and is routed via an additional isolator to an LJPA for phase-sensitive amplification. We double-pump the LJPA symmetrically at $\omega_m \pm \omega_{dp}$ to reduce signal leakage at ω_m. The double pump for the LJPA is generated via an IQ mixer with a third generator operating at $\omega_{dp}/2\pi = 369$ MHz on the I port and a ω_m as the LO. The amplified readout passes through two isolators and a low-pass filter en route to a 4K HEMT; at room temperature, the signal is further amplified before demodulation (using the third branch of ω_m as the LO) and digitization for processing.

CHOOSING AN OPERATING FREQUENCY

As noted in the first section of this Supplement, the output of a double-reflection measurement at measurement frequency ω_m for two 3D transmons with bare cavity frequencies $\omega_{r,1}$ and $\omega_{r,2}$, measurement port bandwidths of $\kappa_{1,2}$, and dispersive shfits $\chi_{1,2}$ is given by the product of two complex reflection coefficients. At steady state, we find:

$$B_{out} = \sqrt{\eta_{loss}} \frac{\frac{\kappa_{s,1}}{2} - i\left(\omega_{r,1} - \omega_m \pm \chi_1\right)}{\frac{\kappa_{s,1}}{2} + i\left(\omega_{r,1} - \omega_m \pm \chi_1\right)} \times \frac{\frac{\kappa_{s,2}}{2} - i\left(\omega_{r,2} - \omega_m \pm \chi_2\right)}{\frac{\kappa_{s,2}}{2} + i\left(\omega_{r,2} - \omega_m \pm \chi_2\right)} A_d \tag{29}$$

For qubits that are red-detuned from the cavities, $+(-)$ corresponds to a qubit in $|0\rangle(|1\rangle)$. We have assumed that $Q_{int} \gg Q_{ext}$, such that we can neglect internal losses. This leads to four distinct resonance curves for the states $|00\rangle$, $|01\rangle$, $|10\rangle$, and $|11\rangle$ (Figure S 2). Solving for the frequency at which $B_{out}^{(10)} = B_{out}^{(01)}$ results in a quadratic equation in ω_m that has real solutions if the following inequality is satisfied:

$$\left(\omega_{r,1} - \omega_{r,2}\right)^2 \geq \left(\frac{1}{4}\frac{\kappa_1\kappa_2}{\chi_1\chi_2} + 1\right)\left[\left(\chi_1 - \chi_2\right)^2 - \frac{\chi_1\chi_2}{\kappa_1\kappa_2}\left(\kappa_1 - \kappa_2\right)^2\right]. \tag{30}$$

Careful manufacture of qubits and cavities enables us to match κ_1 and κ_2 within 2-3 MHz, and χ_1 and χ_2 within several hundred kHz. As a result, this condition is fairly straightforward to meet by adjusting the cavity frequencies such that $|\omega_{r,1} - \omega_{r,2}| \sim \kappa$. It is possible to theoretically calculate the correct ω_m; in practice, we sequentially prepare the computational states $|00\rangle$, $|01\rangle$, $|10\rangle$, and $|11\rangle$, and adjust ω_m until the single-shot Gaussian measurement histograms for the $|01\rangle$ and $|10\rangle$ states completely overlap, as shown in Figure 2 of the main paper.

SYSTEM CALIBRATION

In order to effectively model our two-qubit system, we need to fully characterize it. The necessary calibrations include: qubit lifetime and dephasing time T_1 and T_2; bare cavity frequencies ω_r and linewidths κ; dispersive shifts χ; amplification efficiency η_{meas} and inter-cavity transmission efficiency η_{loss}; measurement photon number $\overline{n_1}$; and gain of the amplification chain G_{chain}. The calibrated values of these parameters are given in Table S1. The calibration methods are described below.

Cavity Frequencies (ω_r) and Linewidths (κ)

The cavity frequencies $\omega_{r,i} + \chi_i$ (that is, the cavity frequency for qubit i in $|0\rangle$) and κ_i are determined via S_{21} measurements at base temperature.

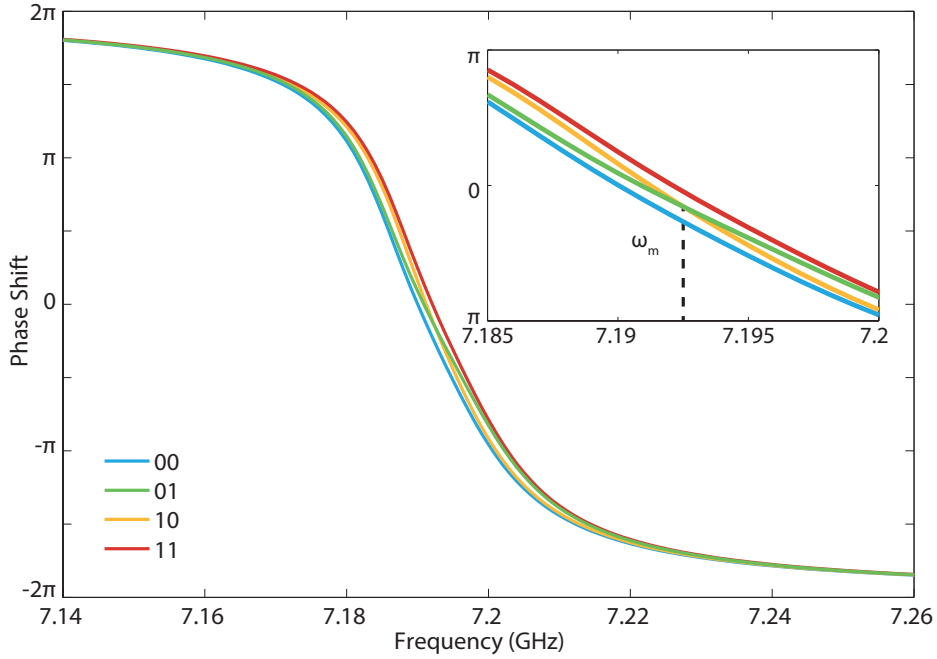

Fig S 2: Double-reflection phase shift calculated for the four prepared states $|00\rangle$, $|01\rangle$, $|10\rangle$, and $|11\rangle$. The reflection curves pass through a 4π, indicating reflection from two sequential cavities. The inset shows the crossing between the reflected phases for $|01\rangle$ and $|10\rangle$ at $\omega_m = 7.19326$ GHz.

Qubit Lifetimes and Coherences

We calibrate T_1 and T_2^* using standard time-resolved measurements.

Photon Number ($\bar{n}_1$), Dispersive Shifts (χ) and Inter-Cavity Transmission Efficiency (η_{loss})

To calibrate χ, η_{loss} and $\bar{n}_1$, we use a technique similar to [5]. We fix a measurement frequency ω_m and perform Ramsey measurements with an additional constant input power P_m (calibrated at room-temperature with a spectrum analyzer), which corresponds to a coherent state in the cavities given by

$$\alpha^{\pm} = \frac{\sqrt{\lambda P_m \kappa}}{\kappa/2 + i\left(\omega_r - \omega_m \pm \chi\right)}, \tag{31}$$

where λ represents an unknown (but constant at fixed frequency) attenuation from room-temperature to the cavity. All variables but χ and λ are independently calibrated. The intracavity coherent state α creates a measurement-induced dephasing rate given by $\Gamma_m = \frac{\kappa}{2}|\alpha^+ - \alpha^-|^2$ and an ac-Stark shift of $\Delta_\omega = -2\chi Re\left[\alpha^-\left(\alpha^+\right)^*\right]$[4]. The frequency of the Ramsey fringes gives Δ_ω, and the exponential decay envelope gives $\Gamma_{tot} = \Gamma_m + 1/T_2^*$. Taking the ratio $\Delta_\omega/\Gamma_{tot} \sim \Delta_\omega/\Gamma_m$ removes dependency on λP_m; we fit this ratio to a constant from which we extract χ. We then use this value of χ in linear fits of $\Delta_\omega(P_m)$ and $\Gamma_m(P_m)$; this provides two independent fits for λ. In Figure 3, we show linear fits for $\Delta_\omega(P_m)$ and $\Gamma(P_m)$ for both qubits, in both instances using readout via the double-reflection measurement such that $\lambda_2 = \lambda_1\eta_{loss}$. This provides our calibration of η_{loss}. The calibration of λ also provides a sensitive photon-number calibration as a function of P_m: once χ and λ have been determined, $\overline{n}^{\pm} = |\alpha^{\pm}|^2$ is fully determined.

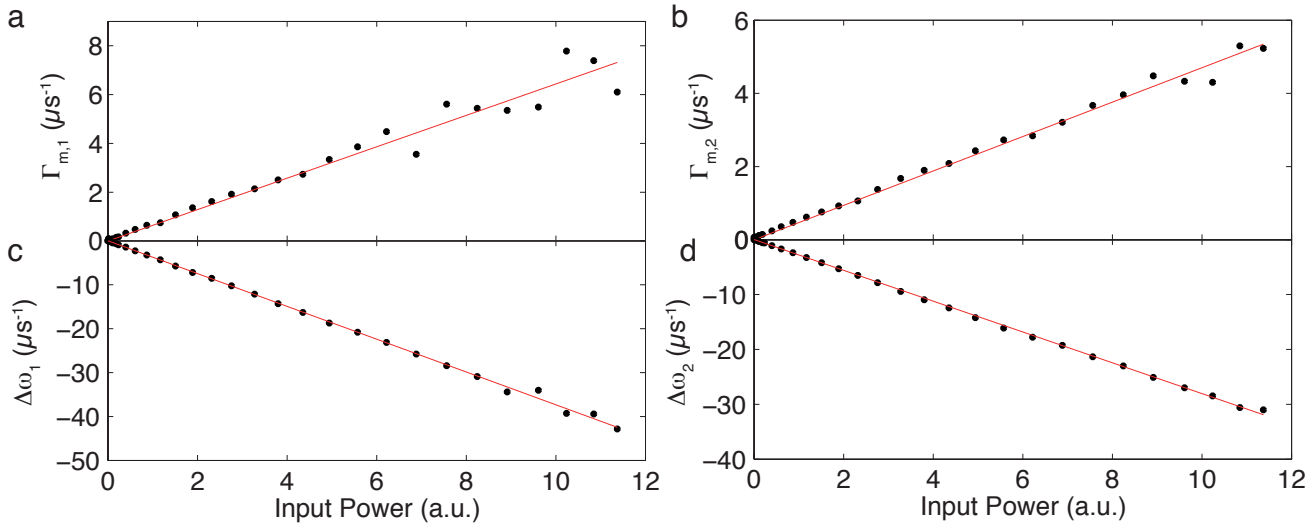

Fig S 3: Measurement-induced dephasing (a-b) and ac-Stark shift (c-d) for qubit 1 (left) and qubit 2 (right) as a function of measurement power P_m in arbitrary units.

Amplification Efficiency (η_{meas}) and Gain of the Amplification Chain (G_{chain})

G_{chain} links the digitized measurement voltage $V_m(t)$ definied in the main paper, and B_{out} as defined in the paragraph "Simplified Theory". G_{chain} is thus the slope of the line $V_m^{(11)} - V_m^{(00)}$ vs $S_{11} - S_{00}$, where V_m^{ij} is the center of the histogram actually measured with the digitizer (Figure S 4), and S_{ij} is defined in Equation 8. Once G_{chain} is determined, we fit the histograms corresponding to the prepared state 00, 01, 10 and 11 (similar to the ones shown in Figure 2 of the main paper) to Gaussian distributions for every measurement time t_m. The amplification efficiency η_{meas} is linked to the standard deviation of these gaussians via $1/\sigma = 2\sqrt{\eta_{meas} t_m}$. We extract η_{meas} by fitting σ vs $1/\sqrt{t_m}$ to a line for every prepared state (See Figure S 4). We define η_{meas} as the mean of these extracted values.

Table S1: System Parameters		
	Qubit 1	Qubit 2
$\omega_q/2\pi$	4.31143 GHz	4.46143 GHz
$\omega_r/2\pi$	7.1864 GHz	7.1984 GHz
$\kappa/2\pi$	18.5 MHz	21 MHz
$\chi/2\pi$	1.275 ± 0.025 MHz	1.085 ± 0.035 MHz
T_1	27 ± 5 μs	20 ± 3 μs
T_2^*	16 ± 3 μs	12 ± 2 μs
η_{loss}	0.81 ± 0.05	
η_{meas}	0.4 ± 0.10	
G_{chain}	19.8 ± 1.6	

TOMOGRAPHY

To tomographically reconstruct the density matrix, we need at least fifteen linearly independent measurements in order to fully determine the 15 degrees of freedom of the two-qubit density matrix. Our tomography procedure utilizes an overspecified set of 30 qubit rotations (15 positive and negative rotations) in order to reduce systematic bias from qubit rotations and power drifts. The rotations are identical to those in Chow et al. [6]. We take advantage of the single-shot nature of our readout to extract the probabilities $p_{|00\rangle}$ and $p_{|11\rangle}$ for each of the 30 rotations, thus doubling the information we gather about the joint qubit state for each measurement. These probabilities represent measurements of the form $\beta_{II}\sigma_{II} \pm \beta_{IZ}\sigma_{Im} \pm \beta_{ZI}\sigma_{nI} + \beta_{ZZ}\sigma_{nm}$, where $+(-)$ corresponds to $p_{|00\rangle}$ $(p_{|11\rangle})$, and $m, n \in \{X, Y, Z\}$. The β-coefficients are calibrated using a double-Rabi measurement as described in Chow *et al*[6]. Our measurement set results in an overspecified measurement set: 60 measurements for 15 degrees of freedom.

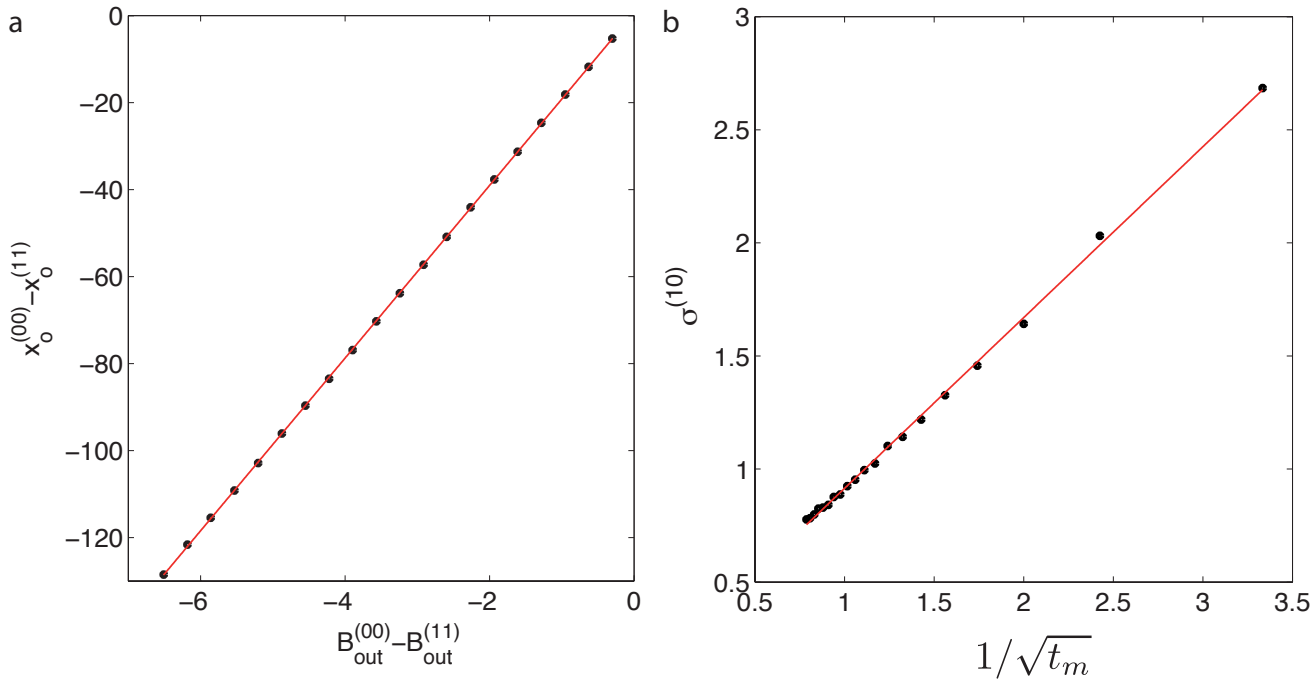

Fig S 4: a. Center of the measured histograms as a function of prediction given by the "simplified theory". We plot the difference between 00 and 11 to get rid of possible offsets. b. Evolution of the standard deviation of the histogram corresponding to prepared state 10 versus measurement time t_m.

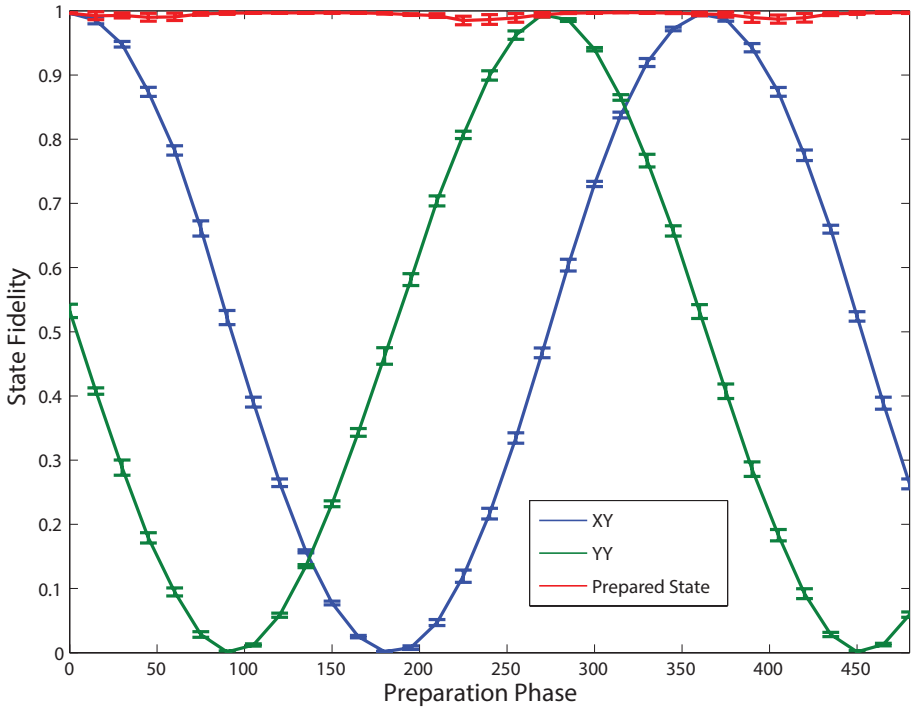

Fig S 5: Fidelity to the states $\frac{|0\rangle+|1\rangle}{\sqrt{2}} \bigotimes \frac{|0\rangle+|1\rangle}{\sqrt{2}}$ (XX), $\frac{|0\rangle+|1\rangle}{\sqrt{2}} \bigotimes \frac{|0\rangle+i|1\rangle}{\sqrt{2}}$ (XY) and $\frac{|0\rangle+|1\rangle}{\sqrt{2}} \bigotimes \frac{|0\rangle+e^{i\phi}|1\rangle}{\sqrt{2}}$ (the Target State) as a function of Qubit 2 preparation phase ϕ. Fidelities to XX and XY oscillate 90 degrees out of phase with one another, as expected; the fidelity to the prepared state is an average of 98.8% across all preparation angles.

We convert this data into a density matrix using a least-squares maximum likelihood estimation method to enforce trace normalization and Hermiticity of the reconstructed density matrix. We verify the accuracy of the tomography by preparing the state $\frac{|0\rangle+|1\rangle}{\sqrt{2}} \bigotimes \frac{|0\rangle+e^{i\phi}|1\rangle}{\sqrt{2}}$ and calcluating the fidelity of the resulting density matrix to the target state (Figure S5). The average fidelity across the prepared states is 98.8%, indicating highly effective state initialization and tomographic reconstruction.

RECONSTRUCTION OF SINGLE QUANTUM TRAJECTORIES

Given a continuous measurement record $V_m(t)$, it is possible to reconstruct the quantum trajectory (time-dependent conditional density matrix) corresponding to it in several ways, as demonstrated in figure 4 of the main paper. In this section we present more details on the various methods for reconstruction.

Reconstruction based on Bayesian update

The Bayesian updating protocol draws on the simplified theory developed in Section 1 of this supplement. For each measurement time t_m, it is possible to infer the density matrix of the two-qubit system by using a Bayesian update based on the measured integrated voltage $V_m(t_m)$ (See for example figure 2.a of the main paper). We first calculate S_{ij} and σ that we recall from Section 1:

$$S_{ij} = \frac{1}{t}\int \mathrm{Re}[B_{out}^{(ij)}(t')\, e^{-i\phi}]\, f_w(t')\, dt', \tag{32}$$

where $f_w(t)$ is the weight function (in the experiment we used constant-weight integration with adjustable start/end time moments). The amplifier noise is also accumulated during this time-integration, so that for the two-qubit state $|ij\rangle$ the random measurement result is characterized by the Gaussian distribution with the mean value of S_{ij} and the standard deviation

$$\sigma = \frac{1}{2\sqrt{\eta_{meas}}}\sqrt{\frac{1}{t}\int f_w^2(t)\, dt}, \tag{33}$$

The selection probability for the initial state $|ij\rangle$ is then given by

$$p_{sel}(i,j) = \int_{V_m-\delta V_m}^{V_m+\delta V_m} e^{-\frac{(V-S_{ij})^2}{2\sigma^2}}\, dV \tag{34}$$

Density matrix elements can then be deduced using equations (11) and (12).

Experimental reconstruction

This reconstruction is based on the ability to map V_m to the actual density matrix. This mapping $V_m \mapsto \rho(V_m)$ is obtained by performing conditional tomography for measurement outcomes lying within the window $[V_m - \delta V_m, V_m + \delta V_m]$ for each measurement time t_m (See figures S6 and S7). To obtain single quantum trajectories, we then just have to superimpose a single realisation of the measurement signal V_m to this experimentally obtained map.

Reconstruction based on stochastic master equation

The conditional density matrix can also be recovered from a measurement trace $V_m(t)$ using the stochastic master equation in Eq. (22). One procedure for this reconstruction is very similar to the experimental reconstruction detailed above. Explicitly, Eq. (22) is simulated for 100000 instantiations of the Wiener noise, a time step of 1ns, and a simulation time of t_m. The homodyne voltage is obtained from the time average of the instantaneous voltage

$$V(t) = \sqrt{\eta_{\mathrm{meas}}}\langle -\sqrt{\kappa_{\mathrm{s},1}\eta_{loss}}\Pi_a + \sqrt{\kappa_{\mathrm{s},2}}\Pi_b]\rangle + \xi(t) \tag{35}$$

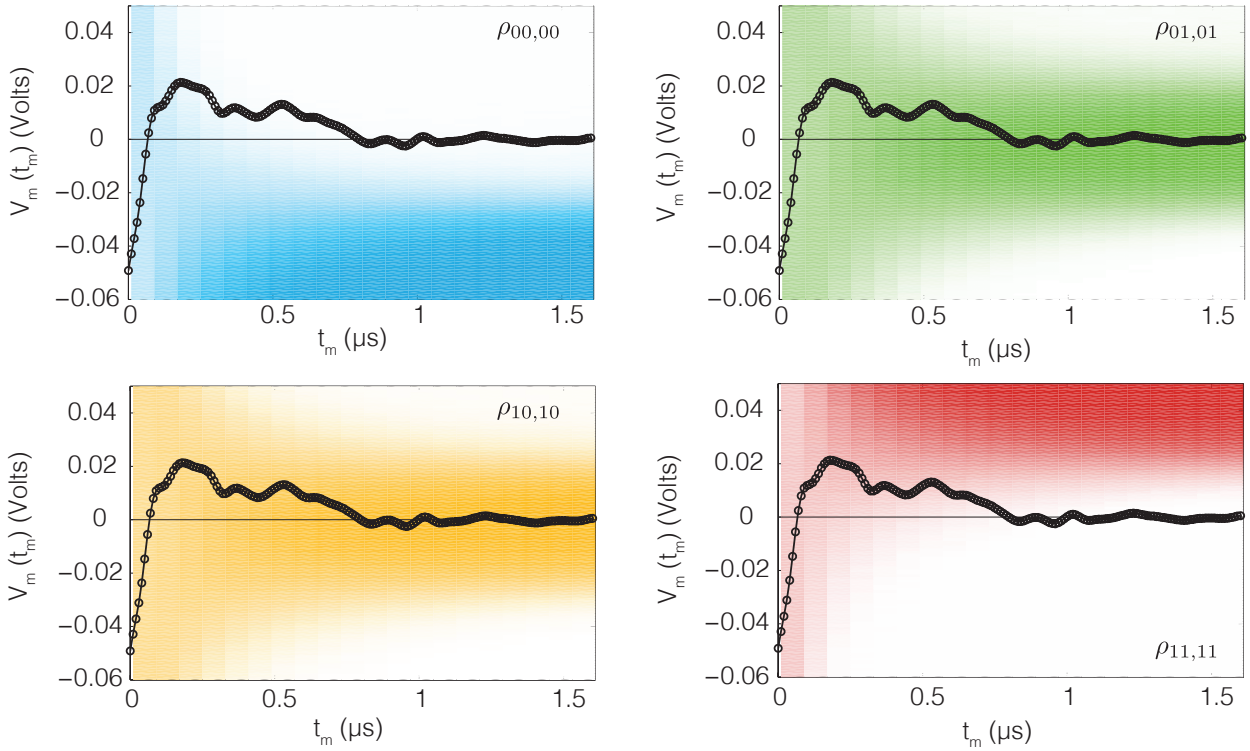

Fig S 6: Diagonal elements of the two-qubit density matrix conditioned on $V_m(t_m)$ and t_m, obtained for $\bar{n} = 1.2$. The color code ranges from 0 (white) to 1 (maximum intensity color). That is, the intensity encodes the estimated value of the density matrix element for a given integrated voltage V_m and measurement time t_m. The dotted line is an example of the temporal evolution of the measurement signal V_m similar to the one on the figure 2.a of the main paper.

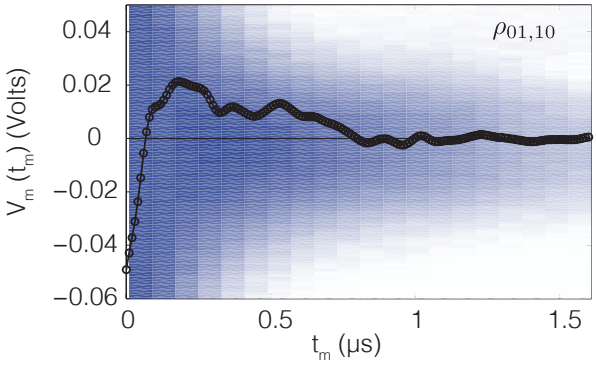

Fig S 7: Absolute value of the off-diagonal element $\rho_{01,10}$ of the two-qubit density matrix conditioned on $V_m(t_m)$ and t_m, obtained for $\bar{n} = 1.2$. The color code ranges from 0 (white) to 1 (maximum intensity color). That is, the intensity encodes the estimated value of the density matrix element for a given integrated voltage V_m and measurement time t_m. The dotted line is an example of the temporal evolution of the measurement signal V_m similar to the one on the figure 2.a of the main paper.

and density matrices conditioned on realizations of the voltage within $[V_m - \delta V_m, V_m + \delta V_m]$ are summed and averaged to give estimates of the conditional density matrix elements.

In principle, it is possible to directly drive the stochastic master equation with the measurement record (*i.e.*, solve Eq. (22) with the experimentally measured $V_m(t)$ substituted). However, for this to produce an accurate trajectory the temporal resolution of the measurement record has to be small ($<$ 1ns) since the stochastic master equation is derived in the infinitesimal time-step limit. This method was not possible in our case because the experimental

apparatus used has a measurement resolution of $\sim$ 10ns.

[1] L. Jakóbczyk and A. Jamróz, Phys. Lett. A **333**, 35 (2004); T. Yu and J. H. Eberly, Phys. Rev. Lett. **97**, 140403 (2006).
[2] A. N. Korotkov, Phys. Rev. B **60**, 5737 (1999);
[3] D. F. Walls, G. J. Milburn, *Quantum optics*, 2nd edition (Springer, 2008).
[4] J. Gambetta, A. Blais, M. Boissonneault, A. A. Houck, D. I. Schuster, and S. M. Girvin, Phys. Rev. A **77**, 012112 (2008).
[5] R. Vijay, C. Macklin, D. H. Slichter, S. J. Weber, K. W. Murch, R. Naik, et al. Nature, **490**(7418), 77–80. (2012)
[6] J.M. Chow, L. Dicarlo, J.M. Gambetta, A. Nunnenkamp, Lev S. Bishop, et al. Phys. Rev. A. **81**, 062325 (2010).
[7] H.J Carmichael. Phys. Rev. Lett. **70**, 2273 (1993).
[8] J. Gambetta, A. Blais, M. Boissonneault, A.A. Houck, D.I. Schuster, & S.M. Girvin. Phys. Rev. A. **77**, 012112 (2008).
[9] F. Motzoi, K. B. Whaley, and M. Sarovar, In preparation (2013).